Hindawi
Geofluids
Volume 2019, Article ID 7320536, 15 pages
https://doi.org/10.1155/2019/7320536

Research Article

Influence of Chemical Corrosion on Pore Structure and Mechanical Properties of Sandstone

Yun Lin[1,2] **Keping Zhou,**[1] **Rugao Gao**[1] **Jielin Li**[1] **and Jian Zhang**[1,2]

[1]*School of Resource and Safety Engineering, Central South University, Changsha, Hunan 410083, China*
[2]*School of Civil, Environmental, and Mining Engineering, University of Adelaide, Adelaide, SA 5005, Australia*

Correspondence should be addressed to Yun Lin; yunlin617@csu.edu.cn, Rugao Gao; gaorgcsu@163.com, and Jielin Li; lijielin@163.com

Received 21 April 2018; Revised 29 September 2018; Accepted 11 November 2018; Published 15 January 2019

Academic Editor: Julie K. Pearce

Chemical corrosion plays a significant role in affecting the properties of rock materials. To understand the effects of chemical corrosion on the pore structure and mechanical properties of sandstones, porosity, T_2 spectrum distribution, and NMR images of sandstone specimens were measured after every 10 days of immersion in chemical solutions using the nuclear magnetic resonance (NMR) technique. Static uniaxial compressive tests and dynamic compressive tests were conducted using a conventional servo-controlled testing machine and a split Hopkinson pressure bar (SHPB) system for specimens treated with chemical corrosion. The test results showed that after being treated with chemical corrosion, the porosity of a specimen increased, the T_2 spectrum distribution would successively shift towards the right, and the distribution of pores tended to become more irregular. Additionally, all of the compressive strength and elastic modulus of sandstone treated with chemical corrosion under static and dynamic loads decreased, and the peak strain increased. The effect order of a chemical solution on the pore structure and mechanical properties of sandstone was H_2SO_4>NaOH>distilled water, which would be related to the different mechanisms of a water-rock reaction. According to the experimental results, the correlations between the mechanical properties and porosity were established. The results can serve as a reference for research in related fields.

1. Introduction

Rock, as a natural geological body, has a pore structure that is closely related to the surrounding environment [1]. Water is one of the most active factors in the environment that affects the porosity of rocks and the safety of rock mass engineering [2, 3]. The change of the microscopic structure and mineral composition of rocks is the essence of a water-rock reaction, which is able to increase the porosity and then affect the physical and mechanical properties of the rock. In recent years, the influence of chemical corrosion on the physical-mechanical properties of rocks has received increasing attention from researchers, especially in the study of large-scale geotechnical engineering problems, such as oil extraction, subgrade, slope, chamber, nuclear waste geological repository, energy underground reservoir, and carbon dioxide geological storage reservoir. A large number of research results have been obtained [3–10].

The effect of chemical corrosion on the pore structure of rocks is time dependent and manifests as the variety of rock porosities with the difference of corrosion time. It is helpful to analyze the corrosion mechanism of chemical solutions and the degradation characteristics of rock mechanical properties to develop the study of the evolution of rock pore structure under the condition of chemical corrosion. Many advanced techniques, such as CT scanning [11–14], SEM [15–18], and *P*-wave velocity [1, 19–21], have been applied to the measurement of pore structures of rocks. These techniques have unique advantages in some aspects, but they cannot be used to obtain the comprehensive effect of chemical corrosion on the pore structure of rocks, such as the distribution and size of pores. Nuclear magnetic resonance (NMR) technology [22, 23], which is a nondestructive spectroscopic testing technique, has been widely used to analyze the internal pore structure of rocks [14, 24–30]. The NMR technique has powerful abilities to obtain the evolution of

the pore structure inside rocks by testing porosity, T_2 spectrum distribution [31], and NMR images [23, 29, 32]. Therefore, the NMR technique is used to investigate the pore structure of rocks in this work.

Rocks exist in a multifield-coupled environment, and many geological disasters of rock mass engineering related to chemical corrosion are caused by the coupling of mechanical action and chemical effect [9, 10]. The deterioration of the static mechanical properties of various rocks treated with different types of chemical corrosion has been widely investigated [4, 11, 33–37]. The mechanical properties which were investigated include UCS, elastic modulus, and Poisson's ratio. These researches were mainly done in the context of static loading conditions. The previous researches mainly focused on the static mechanical properties, and limited studies have been conducted on the dynamic mechanical behaviors of rocks treated with chemical corrosion.

Dynamic stress or impact loads, such as rockbursts, earthquakes, and blasting, have significant effects on the safety and stability of rock engineering, and many rock engineering disasters are caused by dynamic stresses or shocks. Under the action of dynamic loading, the dynamic mechanical behaviors of rocks, such as compressive strength, deformation, and failure process, are quite different from those of rocks under the static state [38–43]. Therefore, it is a very important issue to determine the rock dynamic properties accurately [44]. However, the results of the current limited researches are still far from a complete understanding of the dynamic mechanical behaviors of rocks treated with chemical corrosion.

In this study, to investigate the effect of chemical corrosion on the pore structure and the static and dynamic mechanical properties of sandstone, the NMR technique was applied to detect porosity, T_2 distribution, and NMR images of sandstone specimens. Then, static and dynamic uniaxial compression tests were carried out to determine the static and dynamic UCS and elastic modulus. In addition, correlations of porosity and mechanical properties of sandstone were established based on the experimental data.

2. Materials and Experimental Methods

2.1. Material Preparation. The rock material tested is fine- to medium-grained red sandstone from the subgrade of a road engineering project in Liuyang City, Hunan Province. All samples were cored from an intact sandstone block with a high degree of integrity and uniformity to eliminate interference factors and ensure the reliability of the test results. The X-ray diffraction (XRD) technique was used to detect the mineral components of the sandstone, and the detected results are shown in Table 1. From Table 1, it can be seen that the sandstone is mainly composed of 71% quartz, 15% feldspar, 8% mica, 4% calcite, and 2% chlorite. Note that the results listed in Table 1 are the average of the samples, and the change of mineral components is little due to the high uniformity of the sandstone block. Thus, the effect of the variety of mineral components can be negligible.

As required by the standards of ISRM suggested in [30, 44, 45], cylindrical specimens with a diameter of 50 ± 1 mm were selected. To ensure the roughness of end surfaces less than 0.2 mm and the nonparallelism within ±0.1%, the ends of specimens were polished. To enhance the accuracy of the tests, the specimens with larger discreteness were excluded by comparing the density, longitudinal wave velocity (LWV), and porosity. The mean porosity, density, and LWV of specimens retained were 5.06%, 2.32 g/cm^3, and 2320 m/s, respectively. In general, two sets of specimens were prepared. The specimens of the first set, with a length/-diameter ratio of 2.0, were used in static tests. Specimens of the other set which have a length/diameter ratio of 1.0 were used in dynamic SHPB tests.

Table 1: Mineral composition of sandstone specimen.

Mineral composition	Content (%)
Quartz	71
Feldspar	15
Mica	8
Calcite	4
Chlorite	2
Clay minerals	<1

Rock mass engineering is always in a complex chemical environment where the ionic composition is complex and the pH value varies. In order to investigate the effect of chemical solutions on rock mass in a laboratory environment and simplify the experimental study, three chemical solutions with varying pH values were prepared in this work, i.e., an acidic solution of H_2SO_4 (pH 2.0), distilled water (pH 7.0), and an alkaline solution of NaOH (pH 12.0). There are four test groups, i.e., A, B, C, and D. Each group concluded six specimens (labeled as 4, 5, 6, 7, 8, and 9). The specimens labeled as A, B, and C were immersed in H_2SO_4 solution, distilled water, and NaOH solution, respectively. Specimens from group D represent the natural group.

2.2. Experimental Procedure. In this work, the specific experimental procedure is as follows: (1) The sandstone specimens are prepared. Specimens were cut into cylinders and excluded by comparing the quality, LWV, and porosity, then they were divided into four groups. (2) The chemical solutions are prepared. H_2SO_4 solution (pH 2.0), distilled water (pH 7.0), and NaOH solution (pH 12.0) were prepared, and the specimens from groups A, B, and C were soaked in H_2SO_4 solution, distilled water, and NaOH solution, respectively. (3) NMR tests were conducted. The porosity, T_2 spectrum distribution, and NMR images of the specimens every 10 days of immersion in chemical solutions were tested until the porosity stays unchanged. (4) Mechanical tests were conducted. For all of the groups, the specimens (labeled as 4, 5, and 6) were tested under the static uniaxial compressive loading, and the specimens (labeled as 7, 8, and 9) were tested by the SHPB system. The complete experiment schedule is shown in Figure 1.

2.3. NMR Tests. The principle of nuclear magnetic resonance detection technology is that the atomic nucleus is magnetized by a magnetic field producing a response to the radio

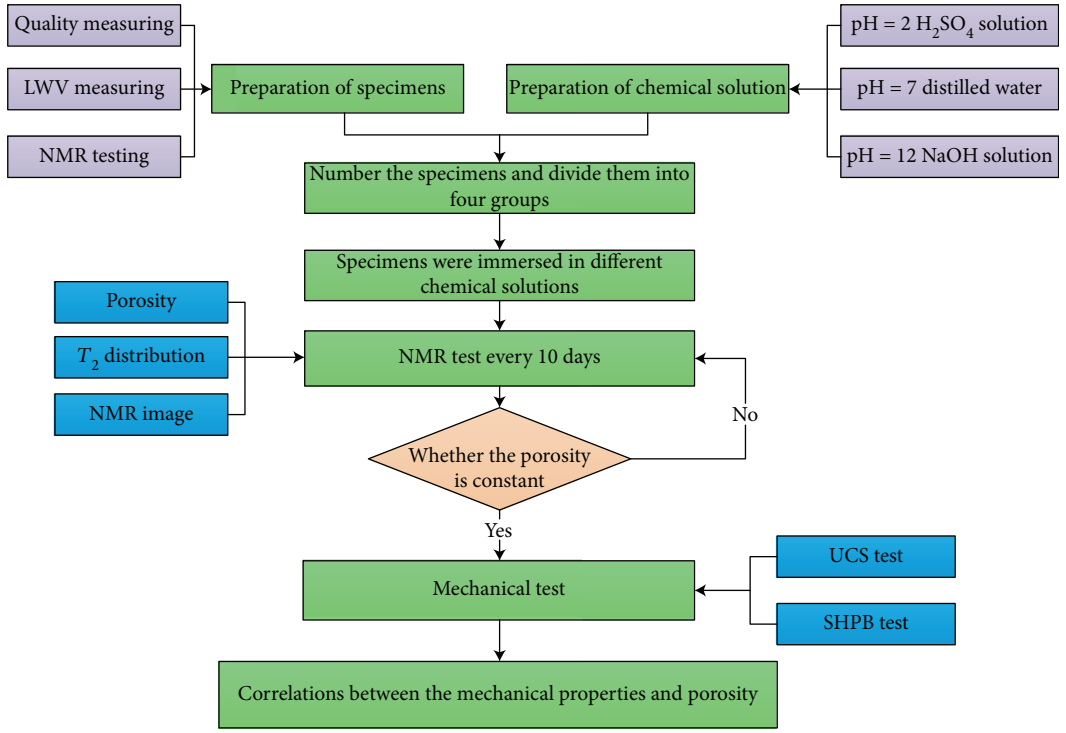

Figure 1: Flow chart of the complete experiment schedule.

frequency; the response can then be reflected by signals that can be measured by the NMR system [23]. Because the rock skeleton has no signal, NMR technology detects the signal of the fluid in the pores of the rocks. When the pores are filled with fluid, the fluid volume is equivalent to the pore volume, so the porosity measured by NMR technology can truly reflect the actual porosity of the rock. The distribution of pores inside the rock is not uniform, and their sizes vary. These result in the different attenuation characteristics obtained in NMR detection. This difference can be expressed by a curve which is called T_2 spectrum distribution. Magnetic resonance imaging is a technique for obtaining the distribution and sizes of pores inside the rock by analyzing the signal attenuation of the atomic nucleus.

The NMR technique has been widely used to measure the porosity, T_2 spectrum distribution, and NMR images of rocks [23, 25–30, 33]. In this work, the AniMR-150 NMR imaging system was used to measure the porosity, T_2 distribution, and NMR images of sandstone specimens every ten days of immersion in chemical solutions (H_2SO_4 solution, distilled water, and NaOH solution).

2.4. UCS and SHPB Tests. To investigate the mechanical behavior of sandstone immersion in chemical solutions, the static and dynamic compressive loading tests were carried out.

The static compression experiments were performed using an Instron-1346 servo-controlled material testing system with a 2000 kN-capacity loading frame. During a test, the axial load and displacement are recorded by a linear variable differential transducer (LVDT). The experiment used the axial displacement control, and specimens were compressed with a loading rate of 0.15 mm/min until failure.

The Splite Hopkinson pressure bar (SHPB) experimental technique is a reliable experimental method for studying the dynamic mechanical properties of materials. The dynamic mechanical tests were carried out on the SHPB test system of Central South University. The schematic of the system is shown in Figure 2. The system consists of a specially shaped striker, an incident bar, a transmission bar, an absorption bar, and a damper. The incident bar, transmission bar, and absorption bar are all 40Cr steel with a longitudinal wave velocity of 5400 m/s, a density of 7810 kg/m^3, and an elastic modulus of 240 GPa [30, 38, 46]. Two strain gauges are attached to the incident and transmission bars to record the deformation of the two bars.

During testing, the gas gun is opened and the specially shaped striker is shot out and impacts the incident bar. Then, an elastic compressive wave is generated and propagates along the incident bar. At the incident bar/specimen interface, the wave is partially reflected and partially transmitted. A portion of the incident wave is reflected back along the incident bar, and the transmission wave propagates along the transmission bar. The strains can be measured with the strain gauges on the bars, stored in digital waveform memory via a dynamic strain gauge, and finally processed by the data processing system.

According to the assumption of 1-D wave propagation [47], the relationship of the stress and strain of the specimen can be calculated as

$$\begin{cases} \sigma(t) = \dfrac{A_b E_b}{2A_s}\left[\varepsilon_i(t) + \varepsilon_r(t) + \varepsilon_t(t)\right], \\ \varepsilon(t) = \dfrac{V_b}{L_s}\displaystyle\int_0^t \left[\varepsilon_i(t) - \varepsilon_r(t) - \varepsilon_t(t)\right]dt, \end{cases} \tag{1}$$

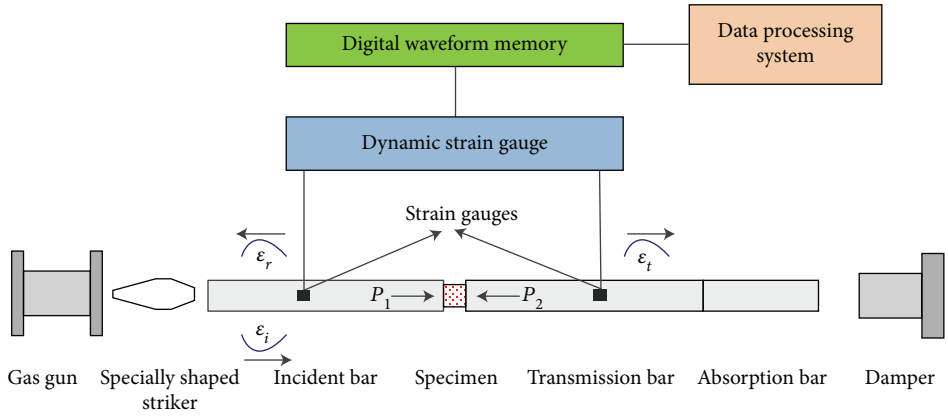

Figure 2: The SHPB test system.

and the forces P_1 and P_2 acting on the specimen shown in Figure 3 can be calculated as

$$\begin{cases} P_1 = A_b E_b[\varepsilon_i(t) + \varepsilon_r(t)], \\ P_2 = A_b E_b \varepsilon_t(t), \end{cases} \tag{2}$$

where V_b, A_b, and E_b represent the wave velocity, the cross-sectional area, and the elastic modulus of the bars, respectively. A_s and L_s are the original area and length of the specimen, respectively. $\varepsilon_i(t)$, $\varepsilon_r(t)$, and $\varepsilon_t(t)$ are the incident strain, reflected strain, and transmission strain, respectively.

3. Evolution of Pore Structure of Sandstones

3.1. Porosity Increment of Specimens under Different Chemical Conditions. The effect of a water-rock reaction on the pore structure of sandstone is time dependent, and the reactions are different with different chemical solutions. In this study, the porosity of specimens was measured by the NMR technique. Since the porosity of specimens from all groups is stable after 50 days of immersion in chemical solutions, the porosity of sandstone specimens with immersion times of 0, 10, 20, 30, 40, and 50 days is shown in Table 2. In order to analyze the variation of porosity more intuitively, the curves of the average porosity of specimens in different chemical solutions are shown in Figure 4.

As Figure 4 displays, the variation of the porosity of sandstone is different with different chemical solutions. When soaked in distilled water, the porosity of sandstone increases significantly in the first 20 days (with an increase rate of 20.77%) and remains unchanged in the last 30 days (with an increase rate of 3.42%). When soaked in H_2SO_4 and NaOH solutions, the characteristics of the two curves are similar. In the first 40 days, the porosity increases obviously and the increase rate decreases with the increase of immersion time. After 40 days of immersion, the curve is almost parallel to the X axis and the porosity tends to be stable. Compared with the curve of specimen immersion in NaOH solution, it can be seen that the increase rate of samples soaked in acid solution is larger, which results in the larger porosity of specimens in the acid solution. Moreover, it also can be concluded that the effect order of chemical solutions on the development of pores inside sandstones is H_2SO_4>NaOH>distilled water.

3.2. T_2 Spectrum Distribution. The characteristics of pore size distribution within the rock can be represented by the curve of the T_2 spectrum. The transverse relaxation time T_2 is positively correlated with pore size, and the signal component corresponding to the peak is correlated with the ratio of the pore [24, 32, 48–50]. The shorter the transverse relaxation time is, the smaller the pore size is, and the larger the signal component corresponding to the peak is, the larger the ratio of the pores with respect to the T_2 time (pore sizes) is.

The curves of T_2 spectrum distribution of sandstone specimens with different times soaked in chemical solutions are shown in Figure 5. From Figure 5, it can be seen that the pores and their size distribution are dynamically changing. The characteristics of pore development inside the rocks are as follows:

(1) There are three peaks (labeled 1, 2, and 3) in T_2 distribution of all the samples at the natural state (without any solutions), indicating that the pore structure of the rock specimens is distributed approximately in three sizes, and the concentrations of the pore distribution in the three sizes are different. It can also be seen that the first two T_2 spectrum peaks of each specimen have a larger porosity component, which means that the number of tiny and medium pores is greater than that of the large pores inside the rock.

(2) When soaked in acid or alkaline solutions, the variation characteristics of the pore structure are different with the increase of soaking time, and the pore structures of specimens change significantly. A new peak appears on the left side of the curve (labeled as peak 4) and the T_2 time is the smallest, indicating that smaller pores (secondary pores) are generated in the specimen caused by chemical corrosion, and the number of secondary pores increases first and then decreases. After 30 days of immersion, the number

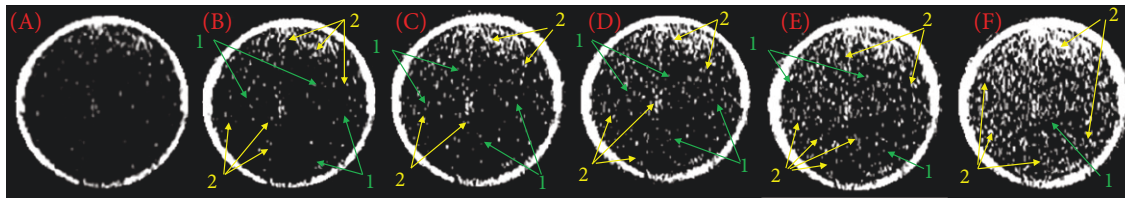

(a) H_2SO_4 solution

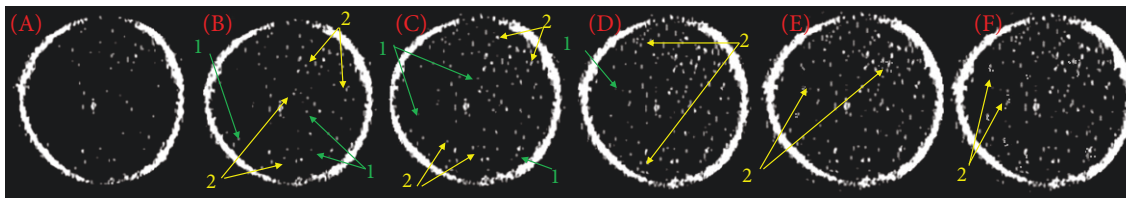

(b) Distilled water

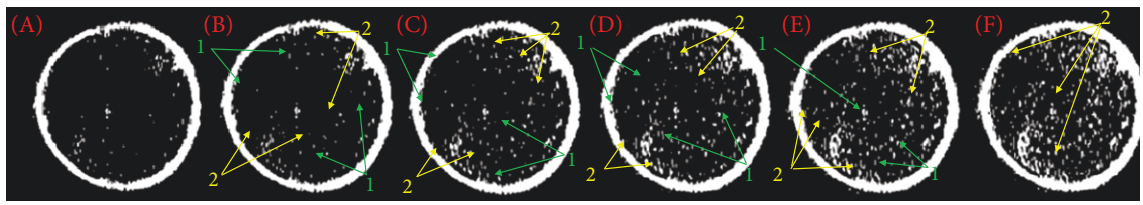

(c) NaOH solution

Figure 3: NMR images of specimens after treatment with different times of chemical corrosion: (A) 0 days; (B) 10 days; (C) 20 days; (D) 30 days; (E) 40 days; and (F) 50 days.

Table 2: Porosity of specimens with different times of immersion in chemical solutions.

Specimen	Porosity of sandstone specimens (%)					
	0 days	10 days	20 days	30 days	40 days	50 days
A4	4.909	6.875	8.590	9.354	9.724	9.819
A5	5.145	7.213	9.011	9.774	10.181	10.235
A6	5.278	7.392	9.265	10.022	10.444	10.561
A7	4.968	6.972	8.684	9.43	9.784	9.996
A8	5.198	7.317	9.109	9.862	10.254	10.416
A9	4.922	6.808	8.595	9.518	9.756	9.863
Average value	5.070	7.096	8.876	9.660	10.024	10.148
B4	5.154	5.822	6.234	6.342	6.390	6.425
B5	5.014	5.682	6.094	6.172	6.216	6.265
B6	5.099	5.787	6.167	6.273	6.326	6.372
B7	4.869	5.517	5.798	5.982	6.015	6.082
B8	5.108	5.772	6.181	6.283	6.339	6.381
B9	5.139	5.807	6.220	6.319	6.373	6.425
Average value	5.064	5.731	6.116	6.229	6.277	6.325
C4	4.950	6.685	7.896	8.521	8.915	9.008
C5	5.134	6.932	8.221	8.831	9.239	9.339
C6	5.137	6.940	8.221	8.836	9.252	9.349
C7	5.062	6.829	8.102	8.714	9.116	9.214
C8	5.158	6.933	8.253	8.876	9.279	9.386
C9	4.943	6.675	7.912	8.506	8.884	8.966
Average value	5.064	6.832	8.101	8.714	9.114	9.210

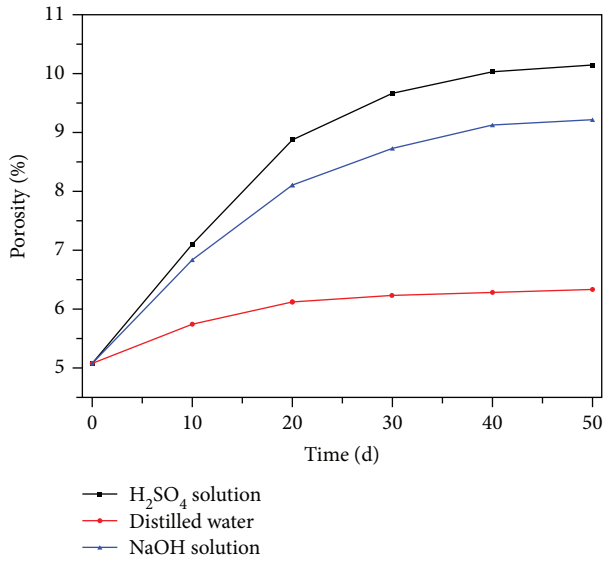

Figure 4: Change curves of average porosity of sandstone specimens with different times of immersion in chemical solutions.

of secondary pores reaches a maximum. The curves shifted to the right with different degrees, and the signal amplitude values are larger than those in the initial state, indicating that the sizes and number of original pores also increase.

(3) In distilled water, the curve of the T_2 spectrum distribution shifted toward the right gradually and the signal amplitude values corresponding to the peaks increase. However, no new peaks are generated. This indicates that the size and number of pores in the sandstone specimen increase under the effect of water dissolution, and no secondary pores are generated inside the specimens

(4) With the increase of soaking time, the signal amplitudes of peaks 1 and 2 on the curves increased significantly, indicating that there is a large increase of tiny and medium pores during the process of the water-rock reaction. These also illustrate the relevance of the evolution of pore size within the specimen. Moreover, it can be drawn that the chemical damage of H_2SO_4 and NaOH solutions is larger than that of distilled water

3.3. Evaluation of NMR Images. The NMR technique can vividly reflect the distribution of pores inside rocks. The NMR image can directly reflect the NMR signal of the fluid that fills the pores, and the distribution and migration of the pore fluid can exactly reflect the development of the pore damage inside the rocks. The bright spots in the images indicate the distribution of pores inside the samples. The larger the bright spot area, the stronger the signal, and the greater the pore volume. Then, the distribution and evolution of pores inside the sandstone specimens can be obtained. The NMR images of sandstone specimens with different times of immersion in different chemical solutions are shown in Figure 3.

There are two types of pores inside specimens with different days of immersion: one is the secondary pore (labeled as ①) and the other one is the pore results from the initial pore size becoming larger (labeled as ②), as shown in Figure 3. From Figure 3, the number and area of light spots increase significantly with the increase of the soaking time, which means that the number and volume of pores inside specimens increase. When soaked in H_2SO_4 solution or NaOH solution, the secondary pores are generated after ten days of immersion, and the number of secondary pores increases with the increase of immersion time in the first 30 days and then decreases in the last 20 days. It can also be seen that the light spots in some areas show a trend of connectivity, but there is no continuity. This indicates that the chemical damage of the area in the rock specimen is serious and the pores are more developed, but there is no macroscopic crack. In addition, the borders of NMR images are obviously brighter. This is mainly because the chemical reaction is related to the contact area, the surface of the specimen is larger in the contact area, and the chemical reaction is more intense than in the internal area. Moreover, the number of NMR images of specimens from groups A and C is larger than that of group B, indicating that the chemical damage of specimens soaked in H_2SO_4 solution and NAOH solution is greater compared with the damage of specimens soaked in distilled water.

In summary, the dissolution and water-rock reaction between the sandstone and H_2SO_4 solution, NAOH solution, and distilled water will cause chemical damage to the sandstone with different degrees, and the order of influence on the pore development within the sandstone is H_2SO_4>NaOH>distilled water.

4. Mechanical Property Deterioration of Sandstone

4.1. Static Mechanical Property of Sandstone. Figure 6 shows the typical uniaxial compressive stress–strain curves of sandstone specimens at different chemical solutions. As shown in Figure 6, four different phases are contained in the typical stress–strain curves: the phase of compaction, the phase of linear elasticity, the phase of plastic yielding, and the phase of failure. The first phase is significant because of the larger porosity of specimens. Moreover, the axil strain corresponding to the peak strength is larger under the condition of chemical immersion, which means that the ductility of sandstone treated with chemical immersion increases. Compared with the failure strain of a specimen under the natural state, the increment of failure strain of sandstone specimens soaked in H_2SO_4 solution is the largest, followed by the increment in NaOH solution, while the increment in distilled water is the smallest.

The results of the static UCS and elastic modulus of sandstone specimens treated with different chemical solutions are shown in Table 3. Figure 7 displays the reductions of the average value of UCS and elastic modulus. Compared with the specimens without any solutions, the chemical damage results in a decrease in the UCS and the elastic modulus.

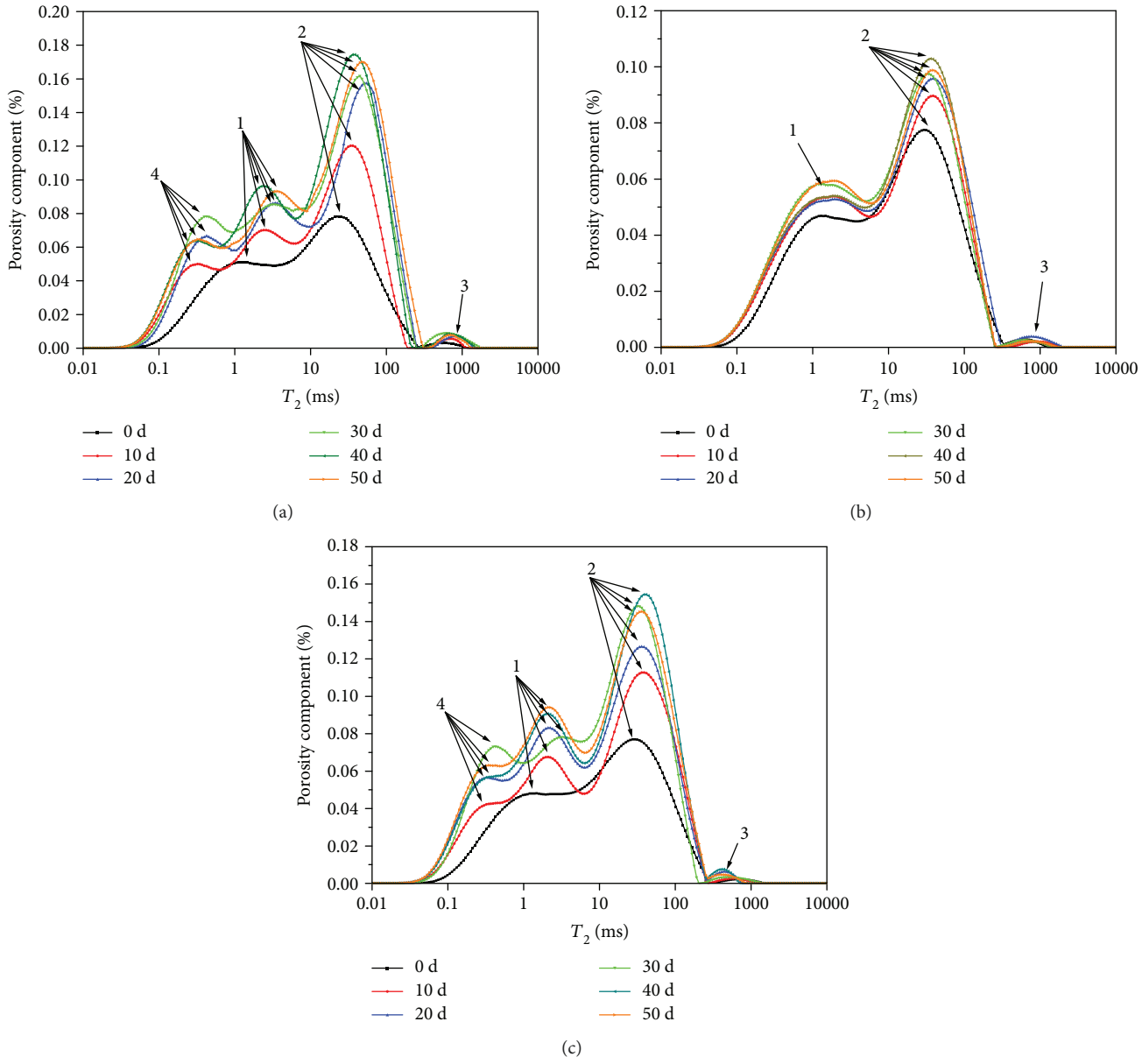

FIGURE 5: T_2 distribution of specimens with different treatment types of chemical corrosion: (a) H_2SO_4 solution; (b) distilled water; and (c) NaOH solution.

After 50 days of immersion in distilled water, NaOH solution, and H_2SO_4 solution, the static UCS was reduced, respectively, to 3.66%, 17.09%, and 18.93%, and the elastic modulus decreased, respectively, by 6.45%, 12.44%, and 15.31%. The reductions have a decisive influence on the stability of practical engineering. The results suggest that the deterioration of static mechanical properties occurs during the reaction between the rock and chemical solutions, and the order of chemical solutions affecting the deterioration of static mechanical properties of sandstones is H_2SO_4>NaOH>distilled water.

Previous studies have indicated that some relations existed between the static mechanical properties and the porosity of sandstones. Based on the experimental data in this study, the relationships between porosity and the static UCS and static elastic modulus are shown in Figure 8. It can be seen that the relationships between porosity and the static mechanical properties of the sandstones are nonlinear. Moreover, exponential function has been experimentally investigated by many scholars [1, 51, 52] to describe the relationship. Therefore, exponential function was also used in this study. The results based on the test data in this study show that equations (3) and (4) fit well on the static UCS and elastic modulus with the fitting coefficient of determination (R^2) of 0.957 and 0.974, respectively.

$$\sigma_s = -80.555 + 158.113e^{-0.018x}, \quad R^2 = 0.957, \tag{3}$$

$$E_s = 8.394 + 8.568e^{-0.296x}, \quad R^2 = 0.974, \tag{4}$$

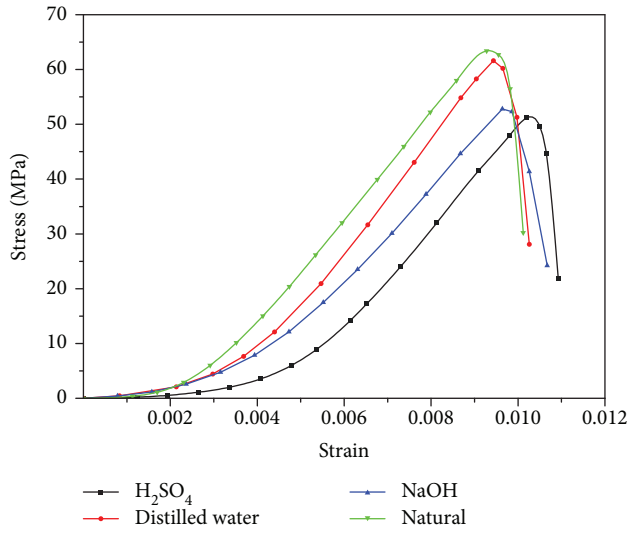

Figure 6: Static stress–strain curves of the sandstone specimens subjected to different chemical solutions.

Table 3: Static uniaxial compression test results for specimens with different chemical solutions.

Specimen group	Number	Static UCS/MPa		Static elastic modulus (GPa)	
		Tested	Average	Tested	Average
H_2SO_4	A7	52.67	51.37	8.76	8.76
	A8	51.15		8.70	
	A9	50.28		8.82	
Distilled water	B7	61.14	61.04	9.73	9.68
	B8	61.62		9.70	
	B9	60.37		9.60	
NaOH	C7	51.13	52.53	9.12	9.06
	C8	52.82		9.00	
	C9	53.65		9.05	
Natural	D7	63.86	63.36	10.45	10.34
	D8	63.43		10.30	
	D9	62.79		10.28	

where σ_s and E_s are the dynamic UCS and elastic modulus, respectively, and x represents the porosity of sandstone specimens.

4.2. Dynamic Mechanical Property of Sandstone. The original and extracted signals of sandstone specimens in a typical SHPB test are shown in Figures 9 and 10. In Figure 9, the signal is continuous and stable and the reflected wave has a good platform segment, indicating that the system is stable and the specimen is in a state of constant strain rate during loading, and the obtained result is reliable. In Figure 10, the transmitted wave (Tr) basically overlaps with the curve of the sum (In + Re) of the incident and reflected waves, indicating that the specimen is basically in the state of stress equilibrium before reaching the peak strength during dynamic loading and the test result is reliable. In addition, the inertial effects are ignored because there is no global force difference in the sandstone specimen to induce inertial forces [38, 46].

The dynamic mechanical parameters are listed in Table 4. By combining Tables 3 and 4, it can be seen that the dynamic strength and elastic modulus are larger than the static strength and elastic modulus of specimens under the same conditions. This may be caused by the specimens that are destroyed instantaneously at the high loading rate.

According to equation (1), the dynamic stress–strain curves of the sandstone specimens treated with different chemical solutions are obtained in Figure 11. The dynamic stress–strain curves can be divided into three phases: the elastic phase, the plastic yielding phase, and the post peak phase. In the first phase, the curve approximately reveals a trend of straight line, which indicates that a compaction still happens but there is only a slow response to the high dynamic load. In the plastic yielding phase, the slope of the curve decreases gradually, which is caused by the continuous mechanical damage of internal materials. At the phase of the post peak, the strength of specimens without any solutions drops rapidly, which means that the effect of the water-rock reaction could weaken the dynamic mechanical capability of the sandstone. Moreover, the slope of stress–strain curves in the phase of elastic and peak stress varies with the different chemical solutions, which results from gradual accumulation of inner chemical damage. The slope and peak stress of specimens without any solutions are the largest, followed by specimens immersed in distilled water, NaOH solution, and H_2SO_4 solution, respectively. Combined with the results of NMR tests, it can be referred that the initial pore size becomes larger and large numbers of secondary pores are generated when the specimens are soaked in chemical solutions, which results in a significant increase of the failure strain of specimens.

Figure 12 displays the reduction of the dynamic compressive strength and elastic modulus of sandstone specimens subjected to different chemical solutions. It can be seen that the original average dynamic compressive strength is 85.79 MPa, and then the dynamic strength reduces to 77.42 MPa, 65.03 MPa, and 60.08 MPa after treatment with corrosion of distilled water, NaOH solution, and H_2SO_4 solution, which are 9.76%, 24.2%, and 29.97% reductions, respectively. Similarly, compared with the original dynamic elastic modulus (30.77 GPa), the reductions of the dynamic elastic modulus are 24.73% (23.16 GPa), 43.81% (17.29 GPa), and 50.76% (15.15 GPa) after 50 days immersion in distilled water, NaOH solution, and H_2SO_4 solution, respectively.

Figure 13 displays the dynamic compressive strength and elastic modulus of samples with different porosities. Based on the experimental data, the relations among porosity, the dynamic compressive strength, and elastic modulus of sandstone are regressed. The results reveal that the exponential functions in equations (5) and (6) fit well with the dynamic compressive strength and elastic modulus with

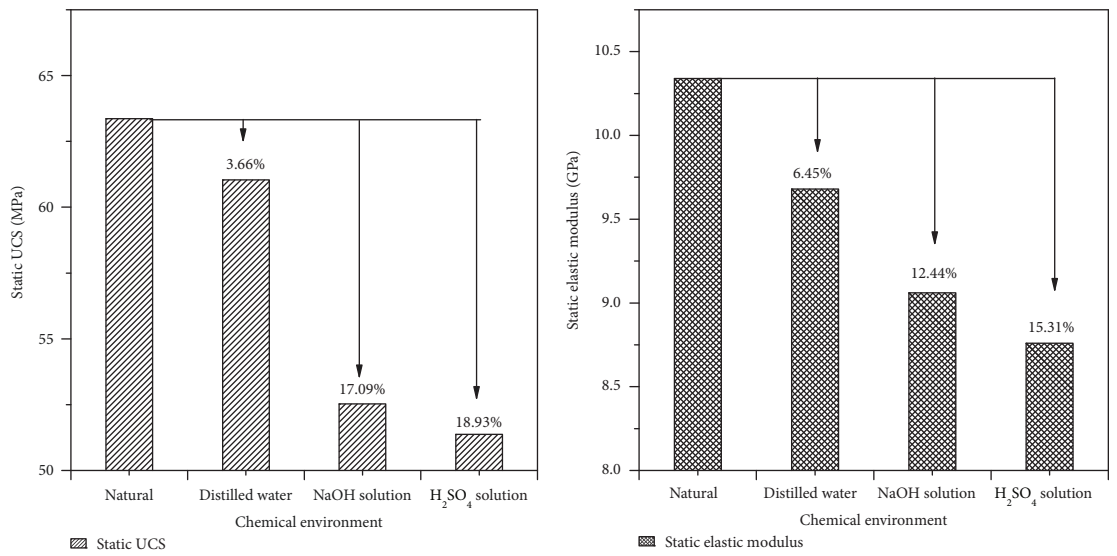

FIGURE 7: Reduction of UCS and elastic modulus for sandstone specimens subjected to different chemical solutions.

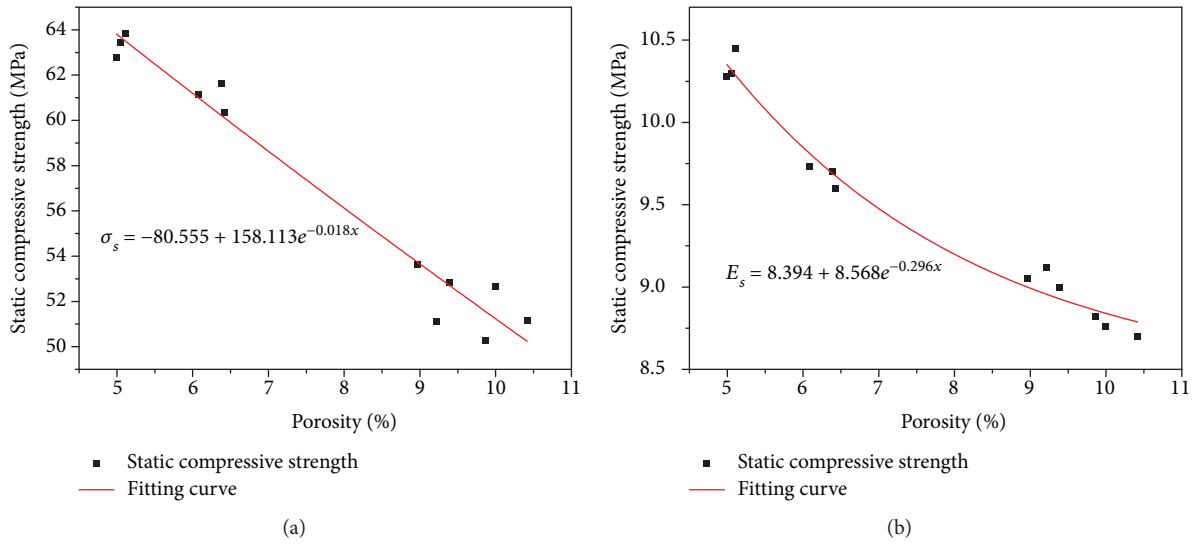

FIGURE 8: Relationship of porosity and static mechanical properties.

the fitting coefficient of determination (R^2) of 0.989 and 0.991, respectively.

$$\sigma_d = 28.554 + 101.347e^{-0.113x}, \quad R^2 = 0.989, \tag{5}$$

$$E_d = 14.167 + 177.824e^{-0.466x}, \quad R^2 = 0.991, \tag{6}$$

where σ_d and E_d are the dynamic compressive strength and elastic modulus, respectively.

4.3. Comparison of Experimental Results and the Proposed Relationships. According to the relationships between porosity and the mechanical properties of sandstones under the static and dynamic states, the static UCS and elastic modulus and dynamic compressive strength and elastic modulus of sandstones treated with different times of immersion in a chemical solution can be predicted. To verity the reliability of the relationships, the experimental data of sandstone specimens (labeled as A10, A11, B10, B11, C10, and C11) treated with 20 days of immersion in a chemical solution was applied. The results are shown in Table 5.

As shown in Table 5, the predicted values are close to the experimental results, and the relative errors are all less than 5%, which indicate that the relationships obtained in this study have good basic prediction capability and are applicable for evaluating the strength of sandstones treated with chemical solutions. However, relative errors still exist. This is because only the porosity could be considered in the

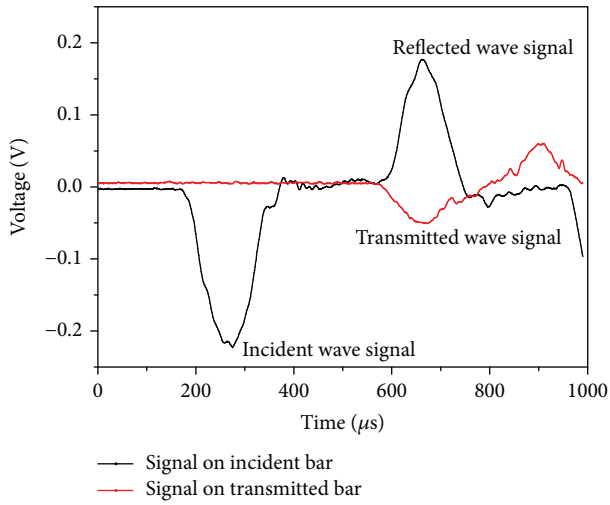

Figure 9: The original signals in a typical SHPB test.

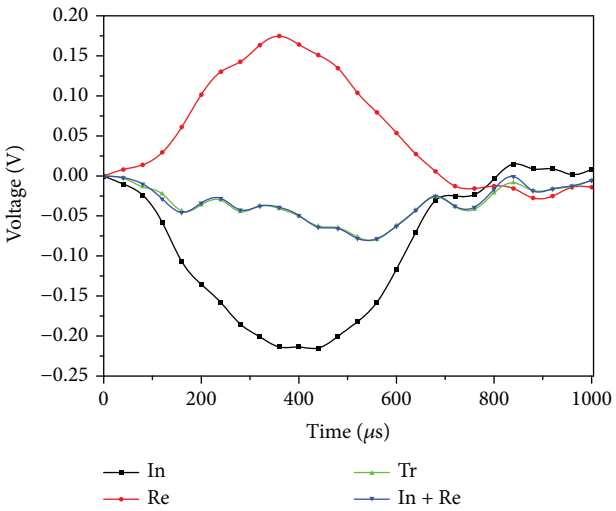

Figure 10: The extracted signals in a typical SHPB test (In, Re, and Tr denote incident, reflected, and transmitted wave, respectively).

Table 4: Dynamic compression test results for specimens with different chemical solutions.

Specimen group	Number	Strength (MPa)		Dynamic elastic modulus (GPa)	
		Tested	Average	Tested	Average
H_2SO_4	A4	61.26	60.08	15.26	15.15
	A5	60.74		15.14	
	A6	58.25		15.06	
Distilled water	B4	78.63	77.42	23.17	23.16
	B5	77.07		23	
	B6	76.57		23.31	
NaOH	C4	66.03	65.03	17.53	17.29
	C5	64.95		17.22	
	C6	64.12		17.12	
Natural	D4	87.03	85.79	30.66	30.77
	D5	85.2		30.89	
	D6	85.14		30.75	

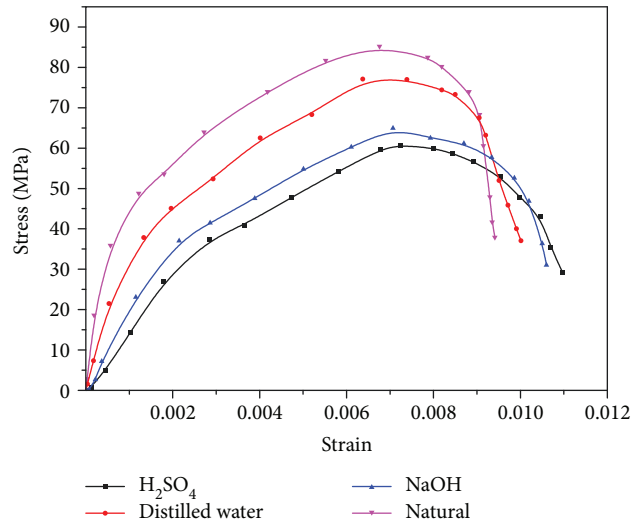

Figure 11: Dynamic stress–strain curves of the sandstone specimens subjected to different chemical solutions.

relationships, but in the test results, all of the factors such as porosity and the distribution and size of pores affect the mechanical properties of the rock. It also can be found that the error rates of specimens treated with immersion in distilled water are the smallest. It may be due to the weak reaction between distilled water and sandstone, which results in weaker pore development inside the rock. These are for future studies.

5. Corrosion Mechanism Analysis

Natural rocks are formed by cemented mineral compounds and internal defects, such as pores and microcracks. At the presence of a chemical solution, the fluid will penetrate into the pores and cracks and interacts with the minerals. Water-rock interactions, including hydrophysical effects and hydrochemical effects, result in the deterioration of rock physical and mechanical properties. In terms of hydrophysical effects, the dissolution of water on rocks reduces the physical and mechanical properties of rocks by reducing the interconnection between the mineral particles and the effectiveness of confining pressure. In terms of hydrochemical effects, the effects deteriorate the physical and mechanical properties of rocks by changing the mineral components and microstructure of rocks, such as the size of particles, pore structures, and crack morphology. The hydrochemical effects are more significant [36], thus the corrosion mechanism of hydrochemical effects are mainly analyzed.

As described in Section 2.1, the sandstone was composed primarily of quartz, feldspar, mica, calcite, and chlorite. When immersed in acid solutions, minerals such as feldspar,

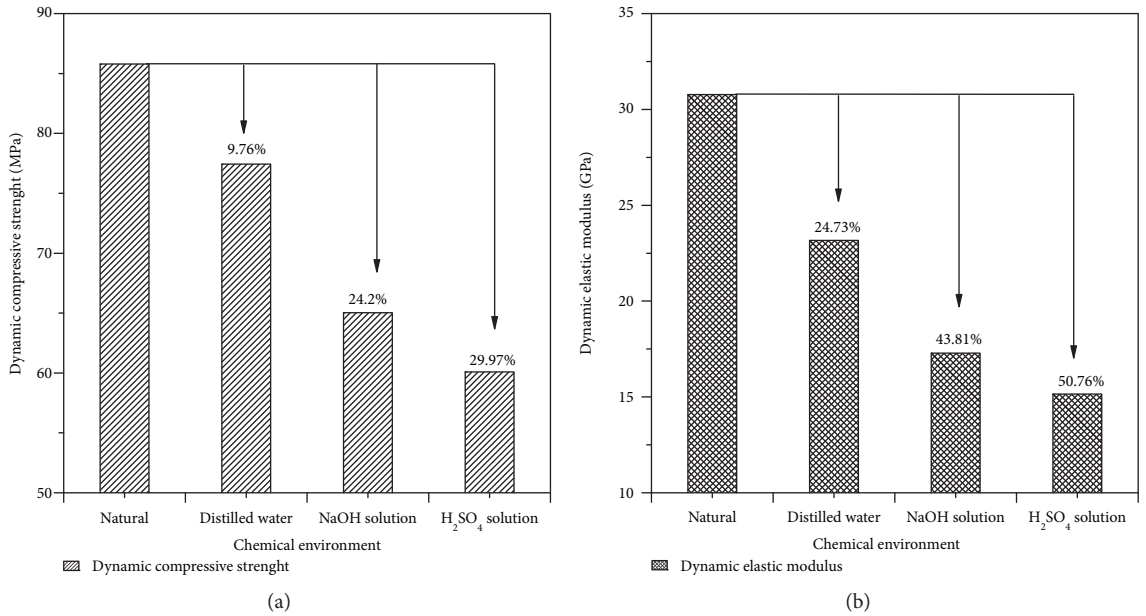

Figure 12: Reduction of dynamic compressive strength and elastic modulus of sandstone specimens subjected to different chemical solutions.

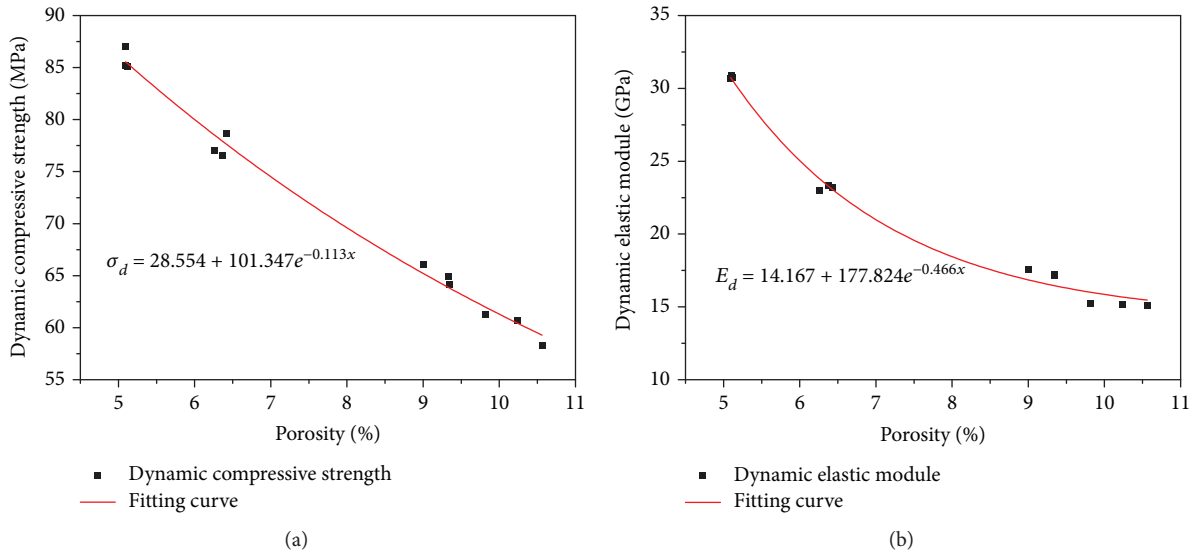

Figure 13: Relationship of porosity and dynamic mechanical properties.

Table 5: Comparison of tested results and predicted values.

Test type	Specimen no.	Porosity (%)	Elastic modulus (GPa)		Error (%)	Compressive strength (MPa)		Error (%)
			Tested	Predicted		Tested	Predicted	
Static mechanical test	A10	8.926	9.19	9.00	2.07%	55.87	54.09	3.19%
	B10	6.132	9.73	9.79	0.62%	61.96	61.03	1.50%
	C10	8.213	9.32	9.15	1.82%	57.34	55.83	2.63%
Dynamic mechanical test	A11	9.013	16.12	16.94	5.09%	67.72	65.51	3.26%
	B11	6.086	25.03	24.38	2.60%	80.92	79.24	2.08%
	C11	8.092	18.87	18.04	4.40%	70.42	68.62	2.56%

calcite, and chlorite can easily react with the hydrogen ion (H^+). Quartz is unstable in alkaline solution. Minerals such as calcite are soluble in water. All of these will result in the change of the physical and mechanical properties of the sandstones. The key corrosion mechanisms for the sandstone studied in this work are summarized below.

When soaked in distilled water, these minerals are not likely to dissolve in water over the experiment timescales. Thus, the corrosion mechanisms of the sandstone treated in distilled water are not analyzed in this study and the detailed reaction equations can be found in the literature [10, 32].

In acidic solution, the main reactions between the major mineral compositions and acidic solution are as follows:

$$\begin{cases} CaCO_3 + 2H^+ \rightarrow Ca^{2+} + H_2O + CO_2\uparrow \\ KAlSi_3O_8 + 4H^+ + 4H_2O \rightarrow Al^{3+} + K^+ + 3H_4SiO_4 \\ NaAlSi_3O_8 + 4H^+ + 4H_2O \rightarrow Na^+ + Al^{3+} + 3H_4SiO_4 \\ KAl_3Si_3O_{10}(OH)_2 + 10H^+ \rightarrow 3Al^{3+} + K^+ + 3H_4SiO_4 \end{cases} \quad (7)$$

Additionally, the mineral composition of sandstone contains chlorite which is active in acid solutions [53, 54], thus the following reactions may also happen when the studied sandstone is soaked in acid solution:

$$Fe_4MgAl_2Si_3O_{10}(OH)_8 + 10H^+ \rightarrow 4Fe^{2+} + Mg^{2+} + Al_2Si_2O_5(OH)_4 + SiO_2 + 7H_2O \quad (8)$$

In alkaline solution, the following reactions mainly occur between the sandstone and the hydroxide ion:

$$\begin{cases} SiO_2 + 2OH^- \rightarrow SiO_3^{2-} + H_2O \\ KAlSi_3O_8 + 6OH^- + 2H_2O \rightarrow 3H_2SiO_4^{2-} + K^+ + Al(OH)_4^- \\ NaAlSi_3O_8 + 6OH^- + 2H_2O \rightarrow Na^+ + Al(OH)_4^- + 3H_2SiO_4{}^{2-} \\ KAl_3Si_3O_{10}(OH)_2 + 8OH^- + H_2O \rightarrow K^+ + 3Al(OH)_4^- + 3SiO_3{}^{2-} \end{cases} \quad (9)$$

Moreover, the concentrations of Ca^{2+}, Na^+, K^+, and SiO_2 were detected in the test and the results are shown in Figure 14. From Figure 14, it can be seen that the ion concentration is dynamically changed under the effect of chemical corrosion. In acid solution, the concentration of Ca^{2+}, Na^+, and K^+ is higher than that in neutral and alkaline solutions. In alkaline solution, the concentration of SiO_2 is higher than that in neutral and acid solutions. These illustrate that different minerals have varying chemical solution sensitivities. Chlorite, feldspar, and calcite (the main component of cement) are unstable in acid solution, and quartz (composition of coarse aggregate) is more active in alkaline solution. The deterioration of the mechanical properties of rocks caused by the dissolution of cement is more significant than that caused by the dissolution of the aggregate [10, 36].

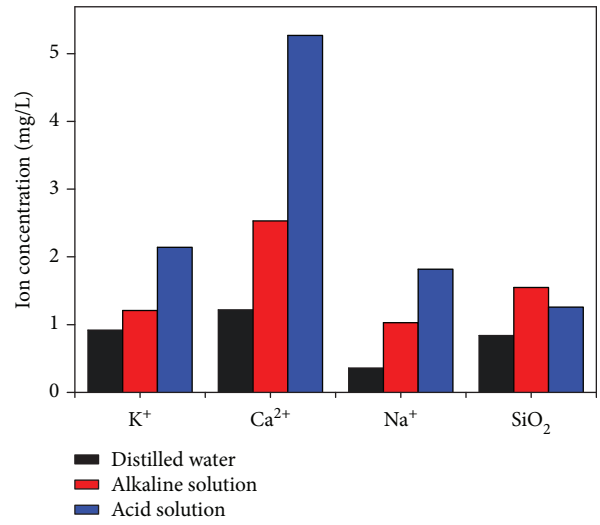

Figure 14: Ion concentrations of chemical solutions after soaking.

Therefore, the chemical corrosion effect of acid solution is more severe compared with that of alkaline and neutral for the sandstone studied.

6. Conclusions

In this study, the alterations on the pore structure and mechanical properties of sandstone caused by chemical corrosion have been experimentally investigated. Based on the experiments, the following conclusions can be drawn:

(1) The pore structure of sandstone treated with chemical corrosion is more developed. When sandstone is soaked in chemical solutions, the porosity increases, the T_2 spectrum distribution shifts towards the right, secondary pores are generated, the pore size becomes larger, and the distribution of pores tends to be more irregular. The effect of H_2SO_4 solution is the greatest, followed by NaOH solution, and distilled water.

(2) The mechanical properties of sandstone treated with different types of chemical corrosion will deteriorate. Under static and dynamic states, the compressive strength and elastic modulus decrease, and the failure strain increases after treatment with chemical corrosion. The corrosion of chemical solutions results in a weakening of the strength and an increase in the ductility of sandstone. The effect order of a chemical solution on the mechanical properties of sandstone is H_2SO_4>NaOH>distilled water, which is due to the larger loss of feldspar and calcite of the sandstone in acid solution and the significant loss of quartz of the sandstone in alkaline solution.

(3) Nonlinear relations existed between the static mechanical properties and porosity of sandstone. The relationships among porosity, the static and dynamic compressive strength, and the static and dynamic elastic modulus were established based on

the experimental data. The porosity is of exponential relation with the static and dynamic mechanical properties. The larger the porosity is, the more reductions of mechanical properties are there.

The results in this work would provide some points to help understand the effects of chemical corrosion on the pore structure and mechanical properties of the sandstones and have a guiding effect on the stability analysis on the subgrade engineering in Liuyang City, Hunan Province. It is also hoped that the results can serve as a reference for research in related fields. However, it should be noted that the mechanical properties of rocks are affected by many factors, such as mineral contents, temperature, and concentration of chemical solutions. Since we did not include these factors in this work, it should be included in future work.

Data Availability

Most of the data generated or analysed during this study are included in this manuscript and all of the data are available from the corresponding author on reasonable request.

Conflicts of Interest

The authors declare that they have no conflicts of interest.

Acknowledgments

The research presented in this paper was jointly supported by the National Natural Science Foundation of China (Grant Nos. 51474252, 51774323, and 41502327), the Project of the State Key Laboratory of Safety and Health for Metal Mines of China (Grant No. 2016-JSKSSYS-02), and the Fundamental Research Funds Project for the Central South University (Grant No. 2016zzts095). The first author would like to thank the Chinese Scholarship Council for financial support to the joint PhD studies at the University of Adelaide.

References

[1] T. Han, J. Shi, and X. Cao, "Fracturing and damage to sandstone under coupling effects of chemical corrosion and freeze–thaw cycles," *Rock Mechanics and Rock Engineering*, vol. 49, no. 11, pp. 4245–4255, 2016.

[2] Y. Lu, L. Wang, X. Sun, and J. Wang, "Experimental study of the influence of water and temperature on the mechanical behavior of mudstone and sandstone," *Bulletin of Engineering Geology and the Environment*, vol. 76, no. 2, pp. 645–660, 2017.

[3] Z. Lu, C. Chen, X. Feng, and Y. Zhang, "Strength failure and crack coalescence behavior of sandstone containing single pre-cut fissure under coupled stress, fluid flow and changing chemical environment," *Journal of Central South University*, vol. 21, no. 3, pp. 1176–1183, 2014.

[4] T. Han, J. Shi, Y. Chen, Z. Li, and C. Li, "Laboratory investigation on the mechanical properties of sandstone immersed in different chemical corrosion under freeze-thaw cycles," *Chinese Journal of Solid Mechanics*, vol. 38, no. 6, pp. 503–520, 2017.

[5] D. Hu, H. Zhou, Q. Hu, J. Shao, X. Feng, and H. Xiao, "A hydro-mechanical-chemical coupling model for geomaterial with both mechanical and chemical damages considered," *Acta Mechanica Solida Sinica*, vol. 25, no. 4, pp. 361–376, 2012.

[6] L. Jiang and Y. Wen, "Damage constitutive model of sandstone during corrosion by AMD," *Journal of Central South University*, vol. 42, pp. 3502–3506, 2011.

[7] A. V. Kiryukhin, E. P. Kaymin, and E. V. Zakharova, "Thermal-hydrodynamic modeling of laboratory tests on the interaction of $NaNO_3$-NaOH fluids with sandstone rock at a deep radionuclide repository site," *Journal of Volcanology and Seismology*, vol. 1, no. 6, pp. 429–438, 2007.

[8] S. Miao, M. Cai, Q. Guo, P. Wang, and M. Liang, "Damage effects and mechanisms in granite treated with acidic chemical solutions," *International Journal of Rock Mechanics and Mining Sciences*, vol. 88, pp. 77–86, 2016.

[9] W. Rühaak, C.-D. Heldmann, L. Pei, and I. Sass, "Thermo--hydro-mechanical-chemical coupled modeling of a geothermally used fractured limestone," *International Journal of Rock Mechanics and Mining Sciences*, vol. 100, pp. 40–47, 2017.

[10] W. Yuan, X. Liu, and Y. Fu, "Chemical thermodynamics and chemical kinetics analysis of sandstone dissolution under the action of dry–wet cycles in acid and alkaline environments," *Bulletin of Engineering Geology and the Environment*, pp. 1–9, 2017.

[11] X.-T. Feng, S. Chen, and H. Zhou, "Real-time computerized tomography (CT) experiments on sandstone damage evolution during triaxial compression with chemical corrosion," *International Journal of Rock Mechanics and Mining Sciences*, vol. 41, no. 2, pp. 181–192, 2004.

[12] R. Peng, Y. Yang, Y. Ju, L. Mao, and Y. Yang, "Computation of fractal dimension of rock pores based on gray CT images," *Chinese Science Bulletin*, vol. 56, no. 31, pp. 3346–3357, 2011.

[13] Y. Wang, X. Li, B. Zhang, and Y. Wu, "Meso-damage cracking characteristics analysis for rock and soil aggregate with CT test," *Science China Technological Sciences*, vol. 57, no. 7, pp. 1361–1371, 2014.

[14] Y. Zhao, G. Zhu, Y. Dong, N. N. Danesh, Z. Chen, and T. Zhang, "Comparison of low-field NMR and microfocus X-ray computed tomography in fractal characterization of pores in artificial cores," *Fuel*, vol. 210, pp. 217–226, 2017.

[15] Z. He, G. Li, S. Tian, H. Wang, Z. Shen, and J. Li, "SEM analysis on rock failure mechanism by supercritical CO_2 jet impingement," *Journal of Petroleum Science and Engineering*, vol. 146, pp. 111–120, 2016.

[16] J. Ni, Y.-L. Chen, P. Wang, S.-R. Wang, B. Peng, and R. Azzam, "Effect of chemical erosion and freeze–thaw cycling on the physical and mechanical characteristics of granites," *Bulletin of Engineering Geology and the Environment*, vol. 76, no. 1, pp. 169–179, 2017.

[17] Y. Zhao, J. Huang, and R. Wang, "Real-time SEM observations of the microfracturing process in rock during a compression test," in *International Journal of Rock Mechanics and Mining Sciences & Geomechanics Abstracts*, pp. 643–652, Elsevier, Pergamon, 1993.

[18] J. Zuo, H. Xie, and H. Zhou, "Investigation of meso-failure behavior of rock under thermal-mechanical coupled effects based on high temperature SEM," *Science China Physics, Mechanics and Astronomy*, vol. 55, no. 10, pp. 1855–1862, 2012.

[19] L. Esteban, L. Pimienta, J. Sarout et al., "Study cases of thermal conductivity prediction from P-wave velocity and porosity," *Geothermics*, vol. 53, pp. 255–269, 2015.

[20] L. A. Lubis, S. Bashah, and D. P. Ghosh, "Comparison of different rock physics models to evaluate the impact of pore types on velocity–porosity relationship in carbonates of Central Luconia Sarawak," in *ICIPEG 2014*, pp. 387–393, Springer, 2015.

[21] G. Pappalardo, "Correlation between P-wave velocity and physical–mechanical properties of intensely jointed dolostones, Peloritani Mounts, NE Sicily," *Rock Mechanics and Rock Engineering*, vol. 48, no. 4, pp. 1711–1721, 2015.

[22] E. C. Gonçalves, P. N. da Silva, C. S. Silveira et al., "Prediction of carbonate rock type from NMR responses using data mining techniques," *Journal of Applied Geophysics*, vol. 140, pp. 93–101, 2017.

[23] J.-l. Li, K.-p. Zhou, W.-j. Liu, and H.-w. Deng, "NMR research on deterioration characteristics of microscopic structure of sandstones in freeze–thaw cycles," *Transactions of Nonferrous Metals Society of China*, vol. 26, no. 11, pp. 2997–3003, 2016.

[24] A. Z. Al-Yaseri, M. Lebedev, S. J. Vogt, M. L. Johns, A. Barifcani, and S. Iglauer, "Pore-scale analysis of formation damage in Bentheimer sandstone with in-situ NMR and micro-computed tomography experiments," *Journal of Petroleum Science and Engineering*, vol. 129, pp. 48–57, 2015.

[25] C. Liu, H. Deng, Y. Wang, Y. Lin, and H. Zhao, "Time-varying characteristics of granite microstructures after cyclic dynamic disturbance using nuclear magnetic resonance," *Crystals*, vol. 7, no. 10, p. 306, 2017.

[26] H. Liu, L. Xiao, F. Deng, W. Chen, and P. Galvosas, "Emerging NMR approaches for characterizing rock heterogeneity," *Microporous and Mesoporous Materials*, vol. 269, pp. 118–121, 2018.

[27] J. Shang, J. Hu, K. Zhou, X. Luo, and M. M. Aliyu, "Porosity increment and strength degradation of low-porosity sedimentary rocks under different loading conditions," *International Journal of Rock Mechanics and Mining Sciences*, vol. 75, pp. 216–223, 2015.

[28] X. Yang, L. Weng, and Z. Hu, "Damage evolution of rocks under triaxial compressions: an NMR investigation," *KSCE Journal of Civil Engineering*, vol. 22, no. 8, pp. 2856–2863, 2018.

[29] K.-p. Zhou, B. Li, J.-l. Li, H.-w. Deng, and F. Bin, "Microscopic damage and dynamic mechanical properties of rock under freeze–thaw environment," *Transactions of Nonferrous Metals Society of China*, vol. 25, no. 4, pp. 1254–1261, 2015.

[30] Z. Zhou, X. Cai, W. Cao, X. Li, and C. Xiong, "Influence of water content on mechanical properties of rock in both saturation and drying processes," *Rock Mechanics and Rock Engineering*, vol. 49, no. 8, pp. 3009–3025, 2016.

[31] J. J. Howard and W. E. Kenyon, "Determination of pore size distribution in sedimentary rocks by proton nuclear magnetic resonance," *Marine and Petroleum Geology*, vol. 9, no. 2, pp. 139–145, 1992.

[32] F. Gao, Q. Wang, H. Deng, J. Zhang, W. Tian, and B. Ke, "Coupled effects of chemical environments and freeze–thaw cycles on damage characteristics of red sandstone," *Bulletin of Engineering Geology and the Environment*, vol. 76, no. 4, pp. 1481–1490, 2017.

[33] Y. Cai, J. Yu, G. Fu, and H. Li, "Experimental investigation on the relevance of mechanical properties and porosity of sandstone after hydrochemical erosion," *Journal of Mountain Science*, vol. 13, no. 11, pp. 2053–2068, 2016.

[34] S. Chen, *Meso—Mechanism and Its Constitutive Model of Rock Damage under Chemical Erosion*, Northeastern University, 2003.

[35] L. Ning, Z. Yunming, S. Bo, and S. Gunter, "A chemical damage model of sandstone in acid solution," *International Journal of Rock Mechanics and Mining Sciences*, vol. 40, no. 2, pp. 243–249, 2003.

[36] L. Qiao, Z. Wang, and A. Huang, "Alteration of mesoscopic properties and mechanical behavior of sandstone due to hydro-physical and hydro-chemical effects," *Rock Mechanics and Rock Engineering*, vol. 50, no. 2, pp. 255–267, 2017.

[37] J. Rutqvist, "Fractured rock stress-permeability relationships from in situ data and effects of temperature and chemical-mechanical couplings," *Geofluids*, vol. 15, no. 1-2, 66 pages, 2015.

[38] B. Ke, K. Zhou, H. Deng, and F. Bin, "NMR pore structure and dynamic characteristics of sandstone caused by ambient freeze-thaw action," *Shock and Vibration*, vol. 2017, Article ID 9728630, 10 pages, 2017.

[39] X. Li, T. Zhou, and D. Li, "Dynamic strength and fracturing behavior of single-flawed prismatic marble specimens under impact loading with a split-Hopkinson pressure bar," *Rock Mechanics and Rock Engineering*, vol. 50, no. 1, pp. 29–44, 2017.

[40] X. Li, Y. Zou, and Z. Zhou, "Numerical simulation of the rock SHPB test with a special shape striker based on the discrete element method," *Rock Mechanics and Rock Engineering*, vol. 47, no. 5, pp. 1693–1709, 2014.

[41] A. Malik, T. Chakraborty, and K. S. Rao, "Strain rate effect on the mechanical behavior of basalt: observations from static and dynamic tests," *Thin-Walled Structures*, vol. 126, pp. 127–137, 2018.

[42] P. Wang, J. Xu, X. Fang, and P. Wang, "Energy dissipation and damage evolution analyses for the dynamic compression failure process of red-sandstone after freeze-thaw cycles," *Engineering Geology*, vol. 221, pp. 104–113, 2017.

[43] L. Weng, X. Li, A. Taheri, Q. Wu, and X. Xie, "Fracture evolution around a cavity in brittle rock under uniaxial compression and coupled static–dynamic loads," *Rock Mechanics and Rock Engineering*, vol. 51, no. 2, pp. 531–545, 2018.

[44] K. Xia and W. Yao, "Dynamic rock tests using split Hopkinson (Kolsky) bar system—a review," *Journal of Rock Mechanics and Geotechnical Engineering*, vol. 7, no. 1, pp. 27–59, 2015.

[45] Z. T. Bieniawski and M. J. Bernede, "Suggested methods for determining the uniaxial compressive strength and deformability of rock materials," *International Journal of Rock Mechanics and Mining Sciences & Geomechanics Abstracts*, vol. 16, no. 2, p. 137, 1979.

[46] Z. Zhou, X. Cai, L. Chen, W. Cao, Y. Zhao, and C. Xiong, "Influence of cyclic wetting and drying on physical and dynamic compressive properties of sandstone," *Engineering Geology*, vol. 220, pp. 1–12, 2017.

[47] G. T. Gray III, "Classic split Hopkinson pressure bar testing," *ASM Handbook, Mechanical Testing and Evaluation*, vol. 8, pp. 462–476, 2000.

[48] A. R. Adebayo, M. E. Kandil, T. M. Okasha, and M. L. Sanni, "Measurements of electrical resistivity, NMR pore size and distribution, and X-ray CT-scan for performance evaluation of

CO_2 injection in carbonate rocks: a pilot study," *International Journal of Greenhouse Gas Control*, vol. 63, pp. 1–11, 2017.

[49] R. F. Sigal, "Pore-size distributions for organic-shale-reservoir rocks from nuclear-magnetic-resonance spectra combined with adsorption measurements," *SPE Journal*, vol. 20, no. 04, pp. 824–830, 2015.

[50] L. Xiao, C. Zou, Z. Mao et al., "An empirical approach of evaluating tight sandstone reservoir pore structure in the absence of NMR logs," *Journal of Petroleum Science and Engineering*, vol. 137, pp. 227–239, 2016.

[51] V. Palchik, "Influence of porosity and elastic modulus on uniaxial compressive strength in soft brittle porous sandstones," *Rock Mechanics and Rock Engineering*, vol. 32, no. 4, pp. 303–309, 1999.

[52] E. Ryshkewitch, "Compression strength of porous sintered alumina and zirconia," *Journal of the American Ceramic Society*, vol. 36, no. 2, pp. 65–68, 1953.

[53] D. E. Clark, I. Gunnarsson, E. S. Aradóttir et al., "The chemistry and potential reactivity of the CO_2-H_2S charged injected waters at the basaltic CarbFix2 site, Iceland," *Energy Procedia*, vol. 146, pp. 121–128, 2018.

[54] J. K. Pearce, D. M. Kirste, G. K. W. Dawson et al., "SO_2 impurity impacts on experimental and simulated CO_2–water–reservoir rock reactions at carbon storage conditions," *Chemical Geology*, vol. 399, pp. 65–86, 2015.